18èmes Journées Internationales de Thermique (JITH 2017)
Monastir (Tunisie), 25 - 27 Octobre 2017

Numerical Study of the offset ratio effect on thermal characteristics of combined wall and offset jet flow

Nidhal Hnaien[1], Saloua Marzouk[1], Habib Ben Aissia[1], Jacques Jay[2]

[1]Unit of metrology and energy systems, National Engineering School of Monastir, Avenue Ibn El Jazzar- 5019 Monastir, Tunisia

[2]Thermal Center of Lyon (CETHIL - UMR CNRS 5008), INSA Lyon, France.

saloua.marzouk@issatgb.rnu.tn, habib_enim@hotmail.fr, jacques.jay@insa-lyon.fr
hnaien_nidhal@yahoo.fr

Abstract

The present paper deals with CFD simulation of a two-dimensional, steady, incompressible and turbulent flow combining a wall jet and an offset jet (this combination will be denoted WOJ: Wall Offset Jet) in order to study the heat transfer phenomenon in this type of flow. Several turbulence models were tested including standard k-ω, SST k-ω, standard k-ε, RNG k-ε and realizable k-ε models. A parametric study was also presented to investigate the offset ratio H and the Reynolds number Re effect on the local (Nu) and average $\left(\overline{\mathrm{Nu}}\right)$ Nusselt number evolution along the wall. Constant wall heat flux boundary condition is considered. The Reynolds number and the offset ratio have been varied respectively from 10000 to 40000 and from 5 to 20 and Pr=0.7 is adopted for all computation. Correlations that predict the average Nusselt number as a function of both the offset ratio H and the Reynolds number Re are also provided. This study has allowed us to conclude that the heat transfer exchanged between the flow and the wall is intensified when decreasing the offset ratio H and increasing the Reynolds number Re.

Keywords: Combined jets, Heat transfer, steady RANS, turbulent flow, vortex center.

1. Introduction

Multi-jet flows play an important role in various industrial applications such as boiler, burners, fuel injection systems, aircraft vertical takeoff and landing, ejectors, heating and air conditioning systems ...etc. The turbulent jets are divided into several categories: the free plane jet, the parallel jets (FPJ: Free Parallel Jets), the offset jet (SOJ: Single Offset Jet), the wall jet (SWJ: Single Wall Jet) and the combination of a wall jet (LWJ: Lower Wall jet) and an offset jet (UOJ: Upper offset jet), the latter combination will be denoted WOJ (Wall Offset Jets) (Fig. 1). The combined wall and offset jets flow (WOJ) is frequently encountered in many industrial process especially in the heat exchanger and the wastewater evacuation process which makes interesting to study the thermal and dynamic characteristics of this type of flow.

The first study on WOJ flow was that of Wang and Tan [1] who have experimentally studied WOJ flow characteristics for a Reynolds number Re=10000 and for an offset ratio H=2 using the PIV (Particle Image Velocimetry) measurement technique. They considered water as working fluid, the flow characteristics such as the average velocity, the shear stress and the half-width at different shear layers are also identified. The flow

statistical characteristics are obtained through an ensemble averaging of 360 instantaneous velocity fields. Wang and Tan [1] have noted the existence of periodical large scale Karman-like vortices in the inner shear layers of the WOJ flow. The existence of the Karman-like vortices result in a periodic interaction between the wall jet (LWJ) and the offset jet (UOJ).

Vishnuvardhanarao and Kumar [2] were studied numerically the heat transfer exchanged between the flow and the wall in the WOJ flow using the standard k-ε turbulence model. The flow is assumed steady and incompressible. The Reynolds numbers considered were taken between 10000 and 40000 and the Prandlt number was Pr=0.7. These authors considered two different thermal boundary conditions at the horizontal wall: constant wall heat flux and constant wall temperature. Vishnuvardhanarao and Kumar [2] have found that far downstream of the nozzles plate, the local Nusselt number Nu increases when increasing either the wall jet (LWJ) or the offset jet (UOJ) initial velocity. They also showed that the local Nusselt number and consequently the heat transfer exchanged between the flow and the wall is higher when considering constant heat flux boundary condition at the horizontal wall. Vishnuvardhanarao and Kumar [2] also noticed that for an offset jet (UOJ) initial velocity of 0.25m/s and that of the wall jet (LWJ) equal to 1m/s, the average Nusselt number reaches maximum value and it is higher by 5% compared to the reference value (the reference value was considered when the UOJ and the LWJ have the same outlet velocity).

The experimental setup of Pelfrey and Liburdy [3] on SOJ flow with a Reynolds number Re=15000 and an offset ratio H=7 was numerically simulated by Kumar [4]. The nozzle width was d=12.5 mm and the nozzle outlet velocity was u_0=17.4m/s. After validating the geometric configuration of Pelfrey and Liburdy [3], Kumar [4] was added in parallel to the offset jet a second wall jet to form a WOJ flow. The purpose of his study was to investigate the wall jet (LWJ) addition effect on the whole WOJ flow structure. The numerical analysis performed by Kumar [4] compares the SOJ flow characteristic to those of WOJ flow for an offset ratio H ranging from 3 to 15 at an interval of 2. It has been shown that the presence of the LWJ parallel to the UOJ result that the UOJ deviates toward the wall and attach to this latter with a higher intensity. This intensity decreases as the offset ratio increases. Correlations that predict the longitudinal and transverse positions of the merge point, combined points and the recirculation vortex centers are also provided according to a single parameter which is the offset ratio H.

Recently, Mondal et al. [5] have numerically investigated the turbulent WOJ flow using unsteady RANS method. In order to validate their numerical model, Mondal et al. [5] have compared their results to those experimental (using PIV technique) of Wang and Tan [1] and numerical (using LES method) of Li et al. [6]. The Reynolds number based on the separation distance between the UOJ and the LWJ is taken equal to Re=10000. The offset jet (UOJ) nozzle width dimensionless by the distance between the two jets is set to 1. On the other hand, the wall jet (LWJ) nozzle is taken between 0.2 and 2. The results show that the merge point longitudinal position decreases as the wall jet width increases while that of the combined point increases. For a LWJ nozzle width equal to 0.2, the WOJ flow remains steady with the existence of two stable counter rotating vortices in the recirculation zone. While, when the LWJ nozzle width is taken between 0.3 and 1, a periodic large scale von Karman-like vortex shedding phenomenon is observed in the same zone.

Through all the work that we have just mentioned, it appears that the majority of WOJ flow studies have mainly focused on determining the positions of the different flow characteristics points such as the merging point, the combined point, the vortices centers and the velocity and pressure fields structure. Except for Vishnuvardhanarao and Kumar [2] who have numerically studied the velocity ratio effect on the heat exchange phenomenon in WOJ flow, there is no significant attempt that has studied the effect of the offset ratio H on thermal characteristics of this type of flow. Thus, the main objective of the present paper is to fill these gaps and to study the simultaneous effect of the offset ratio and the Reynolds number on the thermal characteristics of WOJ flow. This study allowed us to provide correlations predicting the average Nusselt number in different flow zones according to the offset ratio H and the Reynolds number Re. Indeed, these correlations may be useful in a quick estimate of the average Nusselt number which manages the heat transfer phenomenon in this type of flow frequently encountered in several industrial applications.

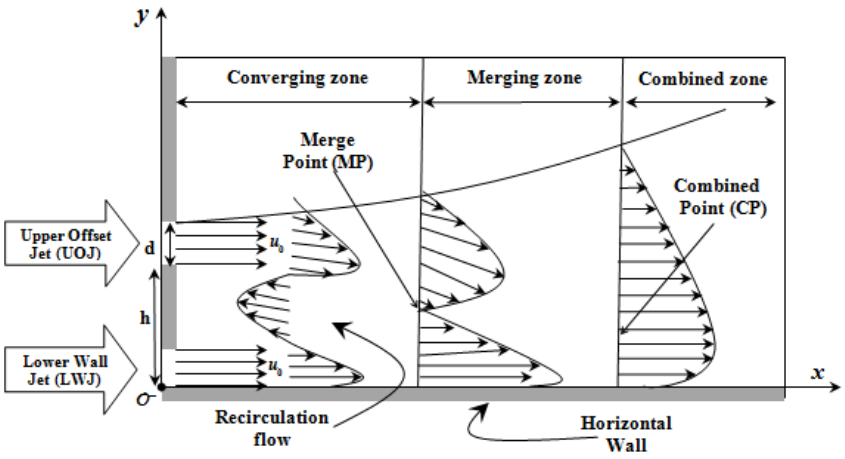

Fig. 1: Combined wall and offset jet flow (WOJ) diagram

2. Mathematical formulations

2.1. Geometric configuration

The geometric configuration of Kumar [4] is used to numerically simulate the offset ratio H effect on thermal characteristics of WOJ flow. As shown in Fig. 2, the wall jet (LWJ) and the offset jet (UOJ) are ejected from two identical and rectangular nozzles each one having d=12.5 mm width and l=150 mm length. The offset ratio H is set to 9, this parameter is defined as the distance between the horizontal wall (defined at y=0) and the offset jet (UOJ) lower extremity. The domain dimensions are chosen so as to not affect the flow propagation. Several configurations were tested before adopting (100×d) and (50×d) dimensions respectively along the longitudinal and the transverse directions.

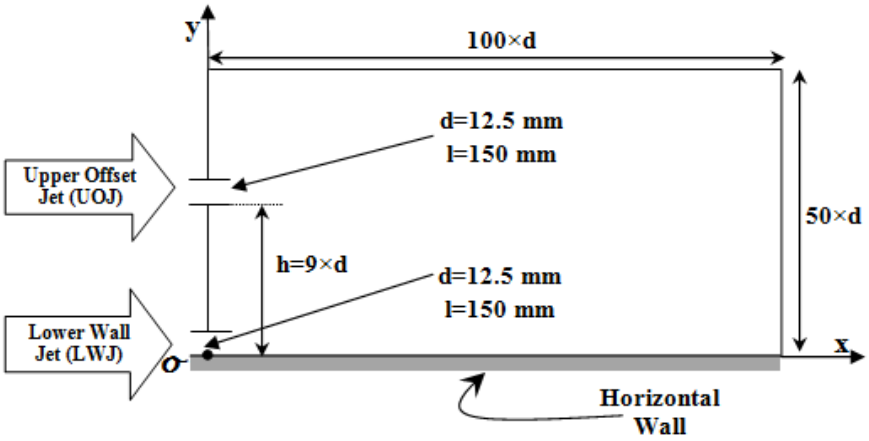

Fig. 2: Combined wall and offset jet flow (WOJ) geometric configuration (Kumar [4]).

2.2. Hypothesis

The equations system governing the flow is written in the Cartesian coordinate system whose origin o is located on the horizontal wall axis (Fig. 2). The following hypothesis will be also adopted:

- The flow is steady and two-dimensional.
- The work fluid is air assumed incompressible and the thermo-physical properties are constant.
- The jets are ejected in the longitudinal direction.
- The flow is assumed to be turbulent and fully developed.

2.3. Governing Equations

The Reynolds-average Navier-Stokes (RANS) equations can be written in Cartesian tensor form as follow:

$$\frac{\partial}{\partial x_i}\left(\rho u_i\right)=0 \tag{1}$$

$$\frac{\partial}{\partial x_j}\left(\rho u_i u_j\right)=-\frac{\partial p}{\partial x_i}+\frac{\partial}{\partial x_j}\left[\mu\left(\frac{\partial u_i}{\partial x_j}+\frac{\partial u_j}{\partial x_i}-\frac{2}{3}\delta_{ij}\frac{\partial u_l}{\partial x_l}\right)\right]+\frac{\partial}{\partial x_j}\left(-\rho\overline{u_i' u_j'}\right) \tag{2}$$

The energy equation is given by the following equation:

$$\frac{\partial}{\partial x_i}\left[u_i\left(\rho E+p\right)\right]=\frac{\partial}{\partial x_j}\left(\lambda_{eff}\frac{\partial T}{\partial x_j}+u_i\left(\tau_{ij}\right)_{eff}\right) \tag{3}$$

The E term is the total energy, λ_{eff} is the effective thermal conductivity and $\left(\tau_{ij}\right)_{eff}$ is the deviatoric stress tensor defined as follow:

$$\left(\tau_{ij}\right)_{eff}=\mu_{eff}\left(\frac{\partial u_j}{\partial x_i}+\frac{\partial u_i}{\partial x_j}\right)-\frac{2}{3}\mu_{eff}\frac{\partial u_k}{\partial x_k} \tag{4}$$

$$\lambda_{eff}=\lambda+\frac{C_p\mu_t}{Pr_t} \tag{5}$$

We note that λ is the thermal conductivity and the default value of the turbulent Prandlt number Pr_t is 0.85. Additional terms now appear which represent the turbulence effect. These Reynolds stresses must be modeled in order to close Eq. (2). One common method employs the Boussinesq approximation to relate the Reynolds stress to the mean velocity gradient as follow:

$$-\overline{\rho u_i' u_j'}=\mu_t\left(\frac{\partial u_i}{\partial x_j}+\frac{\partial u_j}{\partial x_i}\right)-\frac{2}{3}\left(\rho k+\mu_t\frac{\partial u_k}{\partial x_k}\right)\delta_{ij} \tag{6}$$

The turbulent kinetic energy k and its specific dissipation rate ω are obtained from the following equations:

$$\frac{\partial}{\partial x_i}\left(\rho k u_i\right)=\frac{\partial}{\partial x_j}\left(\Gamma_k\frac{\partial k}{\partial x_j}\right)+G_k-Y_k+S_k \tag{7}$$

$$\frac{\partial}{\partial x_i}\left(\rho\omega u_i\right)=\frac{\partial}{\partial x_j}\left(\Gamma_w\frac{\partial \omega}{\partial x_j}\right)+G_\omega-Y_\omega+S_\omega \tag{8}$$

In these equations, G_k and G_ω respectively represent the generation of k and ω due to the mean velocity gradient. Γ_k and Γ_ω are respectively the effective diffusivity for k and ω. Y_k and Y_ω are the dissipation of k and ω due to the turbulence. S_k and S_ω are the source terms. The effective diffusivity for the k-ω model is given by the following equations:

$$\Gamma_k=\mu+\frac{\mu_t}{\sigma_k} \tag{9}$$

$$\Gamma_\omega=\mu+\frac{\mu_t}{\sigma_\omega} \tag{10}$$

$$\mu_t=\alpha^*\frac{\rho k}{\omega} \tag{11}$$

With $\sigma_k=\sigma_\omega=2$ are the turbulent Prandtl numbers respectively for k and ω and α^* is calculated as follow:

$$\alpha^*=\alpha_\infty^*\left(\frac{\alpha_0^*+Re_t/R_k}{1+Re_t/R_k}\right) \tag{12}$$

$$Re_t=\frac{\rho k}{\mu\omega} \tag{13}$$

$$\alpha_0^*=\frac{\beta_i}{3} \tag{14}$$

With $R_k=6$ and $\beta_i=0.072$ are constant values. It is noted that for high Reynolds number k-ω model we have $\alpha^*=\alpha_\infty^*=1$. The terms G_k and G_ω appearing respectively in Eqs. (7-8) are defined by:

$$G_k=-\rho\overline{u_i' u_j'}\frac{\partial u_j}{\partial x_i} \tag{15}$$

$$G_k=\mu_t S^2 \tag{16}$$

$$S\equiv\sqrt{2S_{ij}S_{ij}} \tag{17}$$

$$\alpha=\frac{\alpha_\infty}{\alpha^*}\left(\frac{\alpha_0+Re_t/R_\omega}{1+Re_t/R_\omega}\right) \tag{19}$$

$$G_\omega=\alpha\frac{\omega}{k}G_k \tag{18}$$

We note that $R_\omega = 2.95$, $\alpha_\infty = 0.52$ and $\alpha_0 = 1/9$ are constant values. Re_t and α^* are respectively given by Eqs. (13) and (12). It is also noted that for high Reynolds number k-ω model we have $\alpha = \alpha^* = 1$. The model details are given in FLUENT user's guide.

2.4. Grid distribution and boundary conditions

2.4.1 Grid distribution

A non uniform grid is adopted along the longitudinal and the transverse directions. Indeed, a fine grid is used near the nozzle plate and a little looser further. As shown in Fig. 3, an uniform grid is used for the [A], [B] and [C] segments with a spacing s=0.05. The [D] segment has a non uniform grid with spacing of 0.5 and an expansion ratio e=1.045 which result a nodes number of 280 on these segments ([A], [B], [C] and [D]). For [E] segment, the grid is non uniform with s=0.5 and e=1.0185 which give a nodes number of 200. It is noted that all opposite segments (presented by (') symbol) have the same grid size. Consequently, we obtained a total number of quadratic cells over the entire domain as follow:

$$N_{totale} = (N_A + N_B + N_C + N_D) \times N_E = 280 \times 200 = 56000 \quad (20)$$

It seems important to note that this particular choice of nodes number will be discussed later in the grid size sensitivity test section.

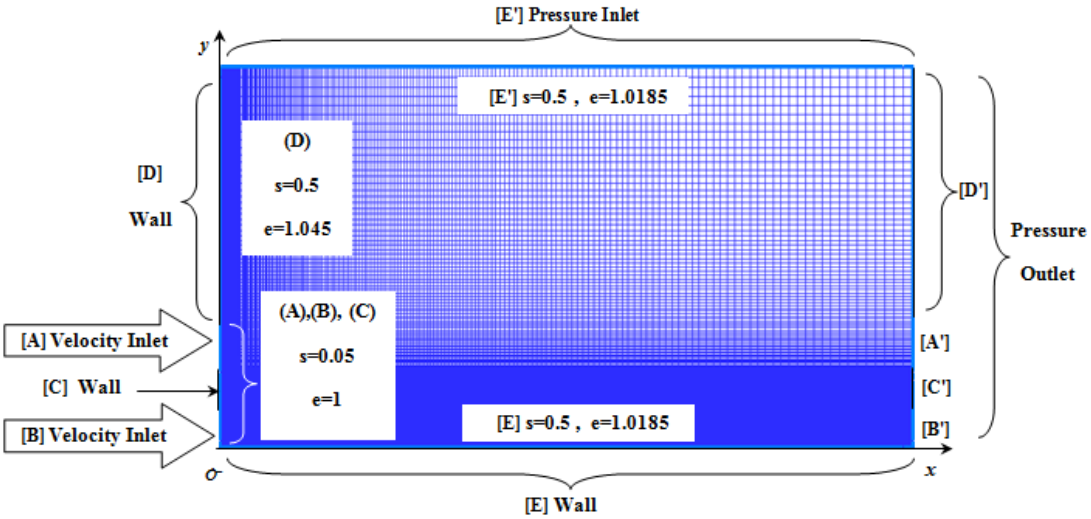

Fig. 3: Mesh and boundary conditions details

2.4.2 Boundary conditions

The boundary conditions (Fig. 3) considered in the present numerical investigation are divided as follows:

- **Velocity Inlet**: This boundary condition is considered at the nozzles exit ([A] and [B] segments) and characterized by uniform velocity profile (u_0=17.4 m/s) giving a Reynolds number Re=15000. Uniform temperature profile with amplitude equal to that of the ambient $(T_0 = T_a = 300K)$ is also considered at the nozzles exit. The turbulence intensity is equal to I=5% [4] giving an initial turbulent kinetic energy $k_0 = \frac{3}{2}(Iu_0)^2 = 1.135\,m^2/s^2$. The turbulent kinetic energy specific dissipation rate ω is given as a function of the turbulent kinetic energy k and the length scale $l = 0.07 \times D_h$ by the following equation $\omega_0 = \frac{k_0^{1/2}}{C_\mu^{1/4} l} = 1203.1 s^{-1}$ with D_h is the hydraulic diameter of the nozzle and $C_\mu = 0.09$ is constant value.
- **Wall**: This condition is considered at the nozzles plate ([C] and [D] segments) and the horizontal wall ([E] segment). For the thermal conditions, this wall ([E] segment) is considered under constant heat flux (q_w=373 w/m²).

- **Pressure Inlet:** Adopted at the free surface boundary at y=50×d ([E] segment). This boundary condition means that the total pressure of the fluid entrained by the flow through this boundary is equal to that of the ambient. The temperature of the entrained fluid is also taken the same as the ambient. The rest of variables will be extrapolated from the solution within the computing domain.
- **Pressure Outlet**: Defined at the flow outlet located at x=100×d ([A'], [B'], [C'] and [D'] segments), this condition is based on the flow pressure at the outlet. All other unknown flow quantities (u, v or T) are calculated from within the computed domain with zero gradients values. This condition allows a rigorous interpolation of the flow variables at the domain outlet.

2.5. Numerical method

The numerical resolution of the transport equations associated to their boundary and exit conditions are solved numerically using the CFD software FLUENT based on the finite volume method developed by Pantakar [7]. The computed region is divided into finite number of sub-regions called "control volume". The resolution method is to integrate on each control volume the transport equations such as the momentum conservation, the mass conservation, the turbulent kinetic energy k, the specific dissipation rate of the turbulent kinetic energy ω and the energy equations. These equations are discretized using the second order upwind. The coupling velocity-pressure is based on the SIMPLEC algorithm. The convergence of the global solution is obtained when the normalized residuals fall below 10^{-4}.

3. Results

3.1. Velocity field validation and grid sensitivity test

Figure 4a shows the transverse distribution of the longitudinal mean velocity U at the plane X=7 using the standard k-ω turbulence model for H=9 and Re=15000. As shown in Fig. 4a, three mesh size were tested such as (180/125), (280/200) and (330/333). These grids contain respectively 22500, 56000 and 109800 quadratic cells. It seems clear that the velocity profile predicted by the mesh size 56000 and 109800 are almost identical while a remarkable difference was found between the prediction by 22500 and 56000 mesh sizes. Thus, the 56000 mesh size is sufficient to obtain a numerical solution independent of the grid size and validated by Kumar [4] results. We showed in Fig. 4b, the same velocity validation with 56000 mesh size using several turbulence models such as the standard k-ω, SST k-ω, standard k-ε, RNG k-ε and realizable k-ε. For $Y \leq 5$, the longitudinal velocity profile predicted by the various turbulence models are in agreement with Kumar [4] results, except the k-ε realizable turbulence models witch over-predicts the velocity profile for $3 \leq Y \leq 5$. While for Y>5 the standard k-ω turbulence model provides the best agreement with Kumar [4] results. Thus, for all computation, we adopt the standard k-ω turbulence model with 56000 mesh size.

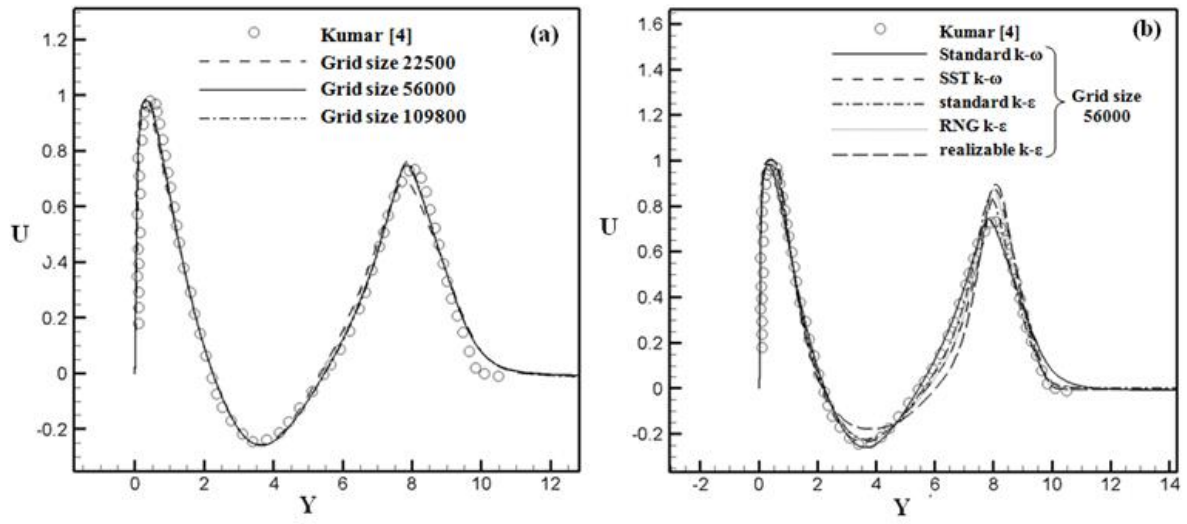

Fig. 4: Longitudinal velocity validation (Kumar [9]) at X=7 for H=9 and Re=15000 (a) grid sizes sensitivity test (b) turbulence models sensitivity test.

3.2. Mean flow structure

The flow combining a wall jet and an offset jet (WOJ flow) is formed by three relevant zones (Fig. 1). The first zone is called the convergence zone wherein the offset jet (UOJ) and the wall jet (LWJ) are attracted towards each other. This zone is characterized by a recirculation flow and a lower pressure due to the training of the fluid existing between the LWJ and the UOJ. The converging zone ends by a point called the merging point (MP) at which the inner shear layers of the LWJ and the UOJ meet. Beyond this merge point, the second zone called the merging zone begins. In this region, the merging process of the two jets take place and ends at a point called the combined point (CP). Beyond this combined point appears the third zone of the WOJ flow, which is the combined zone in which the WOJ flow behaves as a single wall jet.

The flow structure in the converging zone is presented in Fig. 5 with the help of the streamlines and velocity magnitude contours for a Reynolds number Re=15000 and for different offset ratio H=5 (Fig. 5a), H=10 (Fig. 5b), H=15 (Fig. 5c) and H=20 (Fig. 5d). These figures show the centers of two counter rotated vortices rested one above the other in the recirculation zone: an upper vortex center (UVC) in the side of the offset jet (UOJ) and another lower (LVC) in the side of the wall jet (LWJ). These vortices (Fig. 5) are also observed in our previous numerical study (Hnaien et al. [8]) as well as in previous investigations on WOJ flow (Wang and Tan [1], Kumar and Das [9], and Kumar [4, 10]). It seems important to note that the upper and lower vortices sizes increase when increasing the offset ratio H. The same observation is made by Kumar [10] who has remarked that when increasing the offset ratio ($3 \leq H \leq 15$), the vortices dimensions become larger. It is also clear from Fig. 5, that increasing the offset ratio H results an increase in the UVC and the LVC longitudinal positions (X_{uvc} and X_{lvc}). This leads us to conclude that, more the UOJ is far away from the LWJ, the UVC and LVC move further downstream along the longitudinal direction. This longitudinal displacement of the UVC and LVC is also noted in previous numerical investigations such as Hnaien et al. [8] and Kumar [4, 10]).

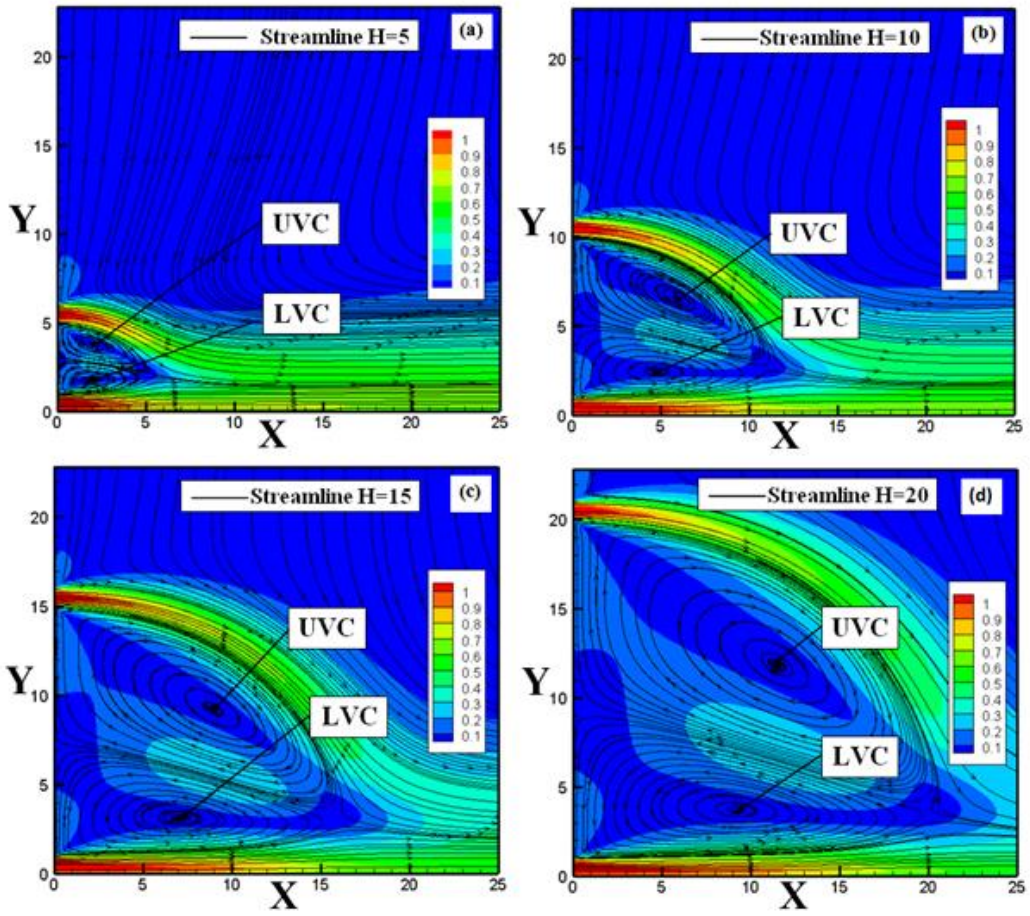

Fig. 5: Streamlines and velocity magnitude contours for Re=15000 and for different offset ratio (a) H=5 (b) H=10 (c) H=15 (d) H=20.

3.3. Local Nusselt number

3.3.1. Converging zone

Figure 6 shows the longitudinal distribution of the local Nusselt number Nu along the converging zone for different Reynolds numbers (10000≤Re≤40000) and offset ratios (5≤H≤20). We note that the local Nusselt number and consequently the local heat transfer increases as the Reynolds number increases. It is also noted that in the vicinity of the nozzle plate (for low X values) the local Nusselt number linearly increases until reaching a maximum value Nu_{max} whose amplitude increases when increasing Re. This allows us to provide the following correlation $Nu_{max} = 0.089\,Re^{0.677}$ that links Nu_{max} to Re. This Reynolds number effect on the maximum Nusselt number is in good agreement with the numerical results of Vishnuvardhanarao and Kumar [2] for WOJ flow with an offset ratio H=2. These authors note that Nu_{max} increase from 40 for Re=10000 to 120 for Re=40000, resulting in an increasing of 200% in the maximum local heat exchange. Moreover, for single offset jet flow (SOJ), Kim and Yoon [11] found that for an offset ratio H=5, the maximum Nusselt number increases with the Reynolds number according to the following correlation $Nu_{max} \propto Re^{0.49}$. In addition, Song et al. [12] proposed two correlations giving the maximum Nusselt number evolution as a function of the Reynolds number $Nu_{max} \propto Re^{0.56}$ and $Nu_{max} \propto Re^{0.65}$ respectively for H=2.5 and H=5. Recently, Gao et al. [13] showed that Nu_{max} increases with the Reynolds number according to the correlation $Nu_{max} \propto Re^{0.77}$ for an offset ratio H=1. We can also note from Fig. 6 that the local Nusselt number Nu for a single wall jet (SWJ) flow (presented by circular symbols) is always higher than that for WOJ flow. This indicates a more intensified heat transfer between the wall and the flow in single wall jet (SWJ) compared to WOJ. This can be explained by the fact that, for the WOJ flow, the offset jet (UOJ) attract the wall jet (LWJ) and try to deviate it away from the wall which subsequently decrease the heat exchanged with the wall. It also clear from Fig. 6 that, in the convergence zone, the local heat transfer increases with the offset ratio H and the maximum heat transfer occurs at the same longitudinal location close to X=2 for all considered Reynolds numbers and offset ratio.

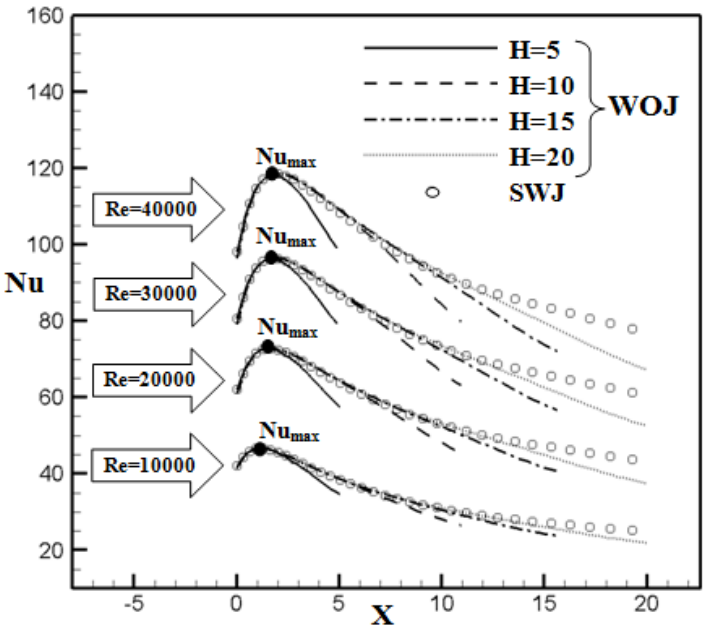

Fig. 6: Longitudinal distribution of the local Nusselt number along the converging zone for different H and Re.

3.3.2. Merging zone

The longitudinal distribution of the local Nusselt number in the merging zone is shown in Fig. 7 for different Reynolds numbers Re and offset ratio H. Analysis of this figure shows that the increase in the Reynolds number produces a rise in the heat transfer for all considered offset ratios. In contrast, for a fixed Reynolds number and for all 5≤H≤20, the local Nusselt number initially longitudinally decreases as the offset height H increases. Then, constant value of Nu appears indicating stabilization in the local heat transfer for some longitudinal positions.

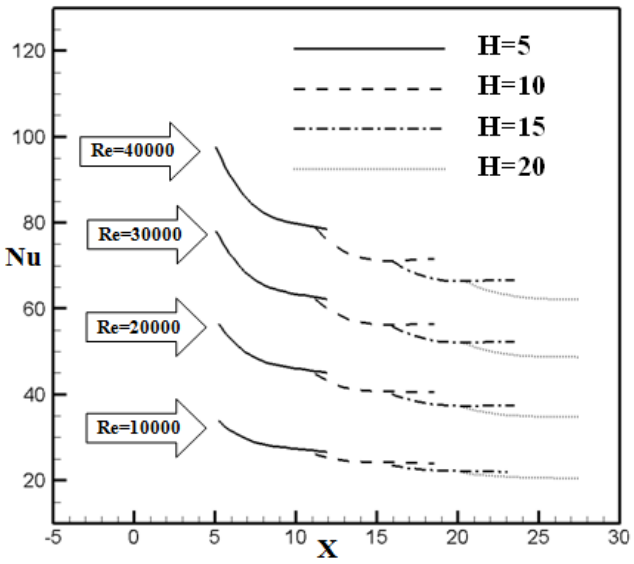

Fig. 7: Longitudinal distribution of the local Nusselt number along the merging zone for different H and Re.

3.3.3. Combined zone

In order to evaluate the heat transfer between the wall and the flow in the combined zone, we present in Fig. 8, the local Nusselt number Nu longitudinal distribution in the final zone of the WOJ flow (combined zone). It is clear from this figure that increasing the Reynolds number leads to an increase in the local heat exchanged between the wall and the flow for all considered offset ratio H. It also noted that for fixed Reynolds number, the local Nusselt number decreases longitudinally following polynomial functions. For longitudinal positions X≤40, the Nu curves are almost identical for all offset ratios H while for longitudinal positions beyond X=40, the increase of H results in a decrease in the local Nusselt number which reflects weakening in the heat transfer. This decay of Nu is little observed for Re=10000, while it becomes more accentuated when the Reynolds number increases.

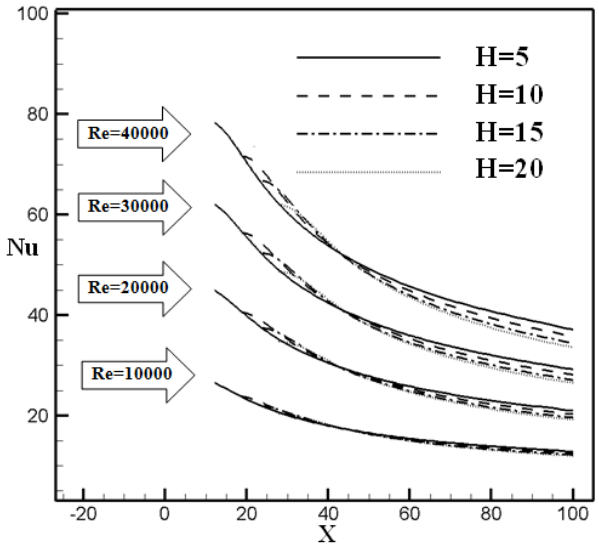

Fig. 8: Longitudinal distribution of the local Nusselt number along the combined zone for different H and Re.

3.4. Average Nusselt number along the wall

To quantify the mean heat exchanged between the flow and the wall under constant heat flux, we defined the average Nusselt number on each flow zone as well as along the whole flow zone as follow:

$$\overline{Nu}_{conv} = \frac{1}{L_{conv}} \int_0^{L_{conv}} Nu dx \qquad (21)$$

$$\overline{Nu}_{merg} = \frac{1}{L_{merg}} \int_0^{L_{merg}} Nu dx \qquad (22)$$

$$\overline{Nu}_{comb} = \frac{1}{L_{comb}} \int_0^{L_{comb}} Nudx \qquad (23)$$

$$\overline{Nu}_{all.zone} = \frac{1}{L} \int_0^{L} Nudx \qquad (24)$$

With L=100×d is the full wall length and L_{conv}, L_{merg} and L_{comb} are respectively the converging, the merging and the combined zones lengths. Fig. 9 presents the average Nusselt number $\overline{Nu}$ evolution along the wall as a function of the Reynolds number Re for different offsets ratio H in the convergence zone (Fig. 9a), the merging zone (Fig. 9b), the combined zone (Fig. 9c) and along the whole flow zone (Fig. 9d). An overview of these curves presented in Fig. 9 shows that the average Nusselt number $\overline{Nu}$ in the different flow zones increases linearly as a function of the Reynolds number for all considered offset ratio H. This Reynolds number effect on the average Nusselt number is also noticed by Vishnuvardhanarao and Kumar [2] in WOJ flow with an offset ratio H=2. These authors noted an increase by 227.4% in $\overline{Nu}$ along the wall when Re increases from 10000 to 40000. Fig. 9 show also that for fixed Reynolds number, the average Nusselt number $\overline{Nu}$ decreases when increasing the offset ratio H. This figure confirms then the previous interpretations concerning the fact that increasing the offset ratio H decreases the heat exchange between the flow and the wall.

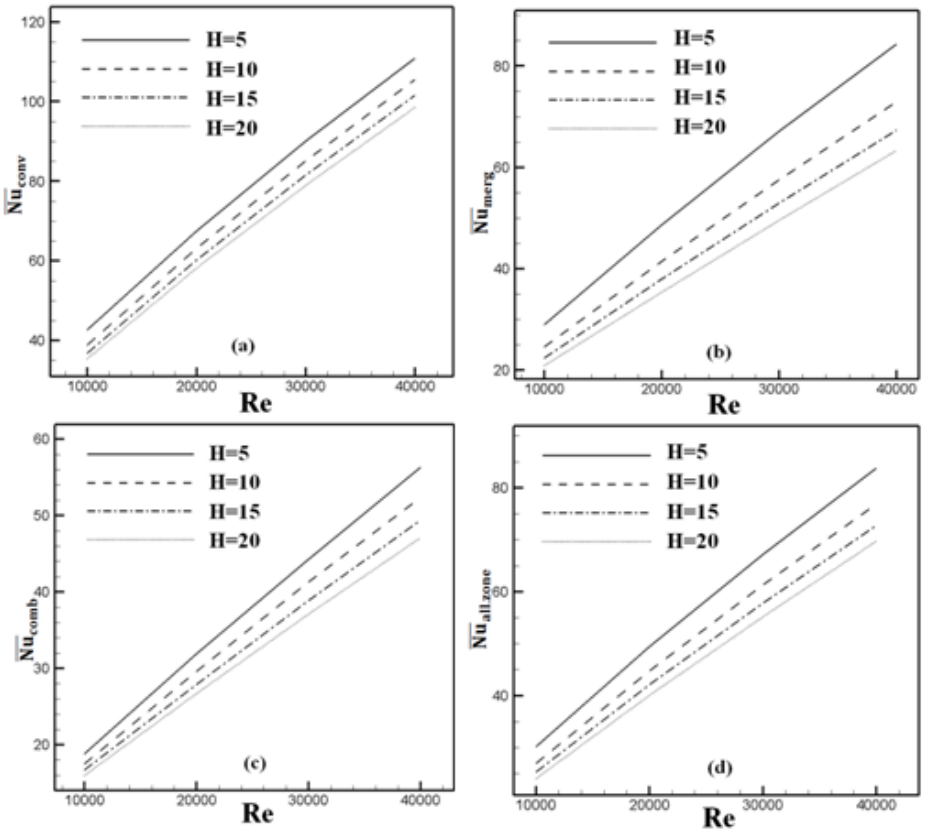

Fig. 9: Average Nusselt number evolution for different H and Re (a) converging zone (b) merging zone (c) combined zone (d) whole flow zone.

3.5. Average Nusselt number estimation

In the previous discussions, we have shown that the Reynolds number Re and the offset ratio H strongly affect the heat transfer along the WOJ flow. Therefore, it is desirable to determine an estimating method of the heat exchanged between the flow and the wall under constant heat flux. In this regard, empirical correlations are proposed to predict heat exchange phenomenon in the convergence, merging and combined zones and along the whole WOJ flow zone.

Fig. 10 shows the scatter plots relative to $Ln\left(\frac{\overline{Nu}_{conv}}{H^{-0.1}}\right)$ (Fig. 10a), $Ln\left(\frac{\overline{Nu}_{merg}}{H^{-0.2}}\right)$ (Fig. 10b), $Ln\left(\frac{\overline{Nu}_{comb}}{H^{-0.13}}\right)$ (Fig. 10c) and $Ln\left(\frac{\overline{Nu}_{all.zone}}{H^{-0.15}}\right)$ (Fig. 10d) curves as a function of $Ln(Re)$ respectively in the converging zone, the

merging zone, the combined zone and in the whole flow zone. These scatters plots may be approximated by the following linear functions:

$$\mathrm{Ln}\left(\frac{\overline{\mathrm{Nu}}_{\mathrm{conv}}}{\mathrm{H}^{-0.1}}\right)=0.716\mathrm{Ln}\,\mathrm{Re}-2.712 \qquad (25)$$

$$\mathrm{Ln}\left(\frac{\overline{\mathrm{Nu}}_{\mathrm{merg}}}{\mathrm{H}^{-0.2}}\right)=0.788\mathrm{Ln}\,\mathrm{Re}-3.623 \qquad (26)$$

$$\mathrm{Ln}\left(\frac{\overline{\mathrm{Nu}}_{\mathrm{comb}}}{\mathrm{H}^{-0.13}}\right)=0.791\mathrm{Ln}\,\mathrm{Re}-4.149 \qquad (27)$$

$$\mathrm{Ln}\left(\frac{\overline{\mathrm{Nu}}_{\mathrm{all.zone}}}{\mathrm{H}^{-0.15}}\right)=0.757\mathrm{Ln}\,\mathrm{Re}-3.359 \qquad (28)$$

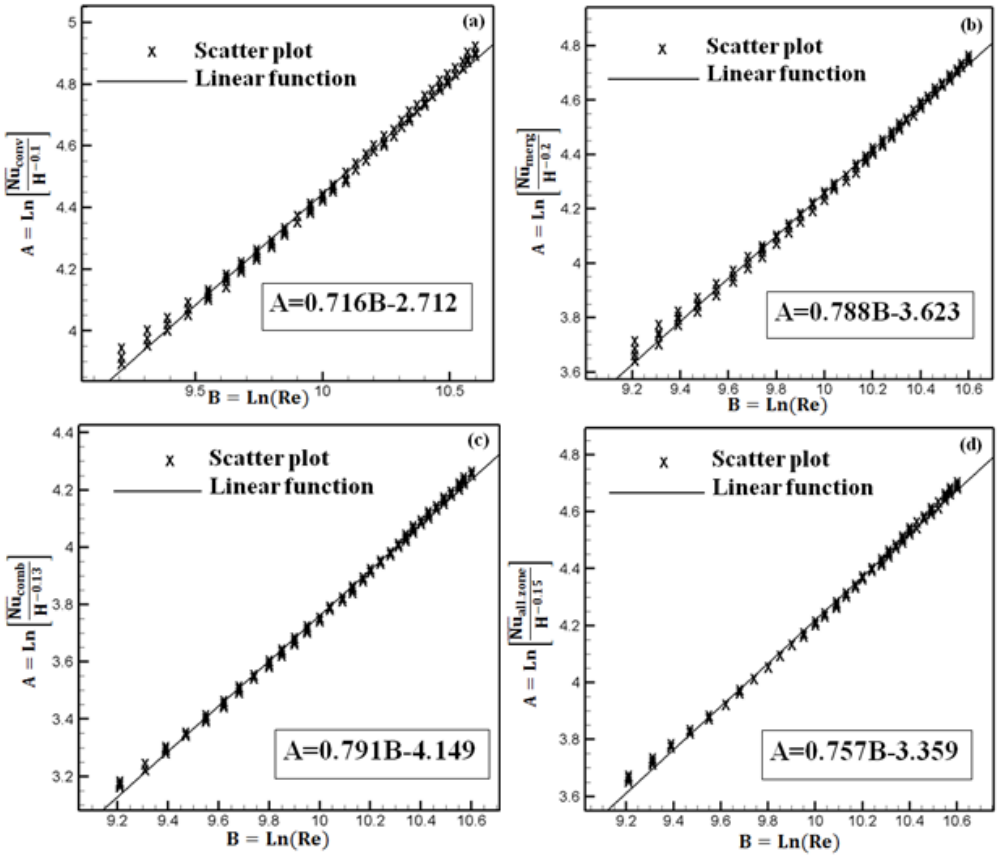

Fig. 10: Scatter plots relative to the average Nusselt number (a) converging zone (b) merging zone (c) combined zone (d) whole flow zone.

Equations (25-28) allow us to deduce the following correlations that predict the average Nusselt number $\overline{\mathrm{Nu}}$ evolution depending on the Reynolds number Re and the offset ratio H:

$$\overline{\mathrm{Nu}}_{\mathrm{conv}}=0.066\mathrm{H}^{-0.1}\,\mathrm{Re}^{0.716} \qquad (29)$$

$$\overline{\mathrm{Nu}}_{\mathrm{merg}}=0.027\mathrm{H}^{-0.2}\,\mathrm{Re}^{0.788} \qquad (30)$$

$$\overline{\mathrm{Nu}}_{\mathrm{comb}}=0.016\mathrm{H}^{-0.13}\,\mathrm{Re}^{0.791} \qquad (31)$$

$$\overline{\mathrm{Nu}}_{\mathrm{all.zone}}=0.035\mathrm{H}^{-0.15}\,\mathrm{Re}^{0.757} \qquad (32)$$

These correlations are valid for a wide range of Reynolds numbers ($10000\leq \mathrm{Re}\leq 40000$) and offset ratios ($5\leq \mathrm{H}\leq 20$). In order to ensure correlations validity and to trust our results, the average Nusselt numbers predicted by Eqs. (29-32) are compared in Fig. 11 to the numerical values already presented in Fig. 9. Our correlations provided by Eqs. (29-32) predict the average Nusselt number in the different flow zones and along the whole flow zone $\overline{\mathrm{Nu}}_{\mathrm{conv}}$, $\overline{\mathrm{Nu}}_{\mathrm{merg}}$, $\overline{\mathrm{Nu}}_{\mathrm{comb}}$ et $\overline{\mathrm{Nu}}_{\mathrm{all.zone}}$ respectively with an average error of 1.5% , 1.3%, 1.1% and 1.2%.

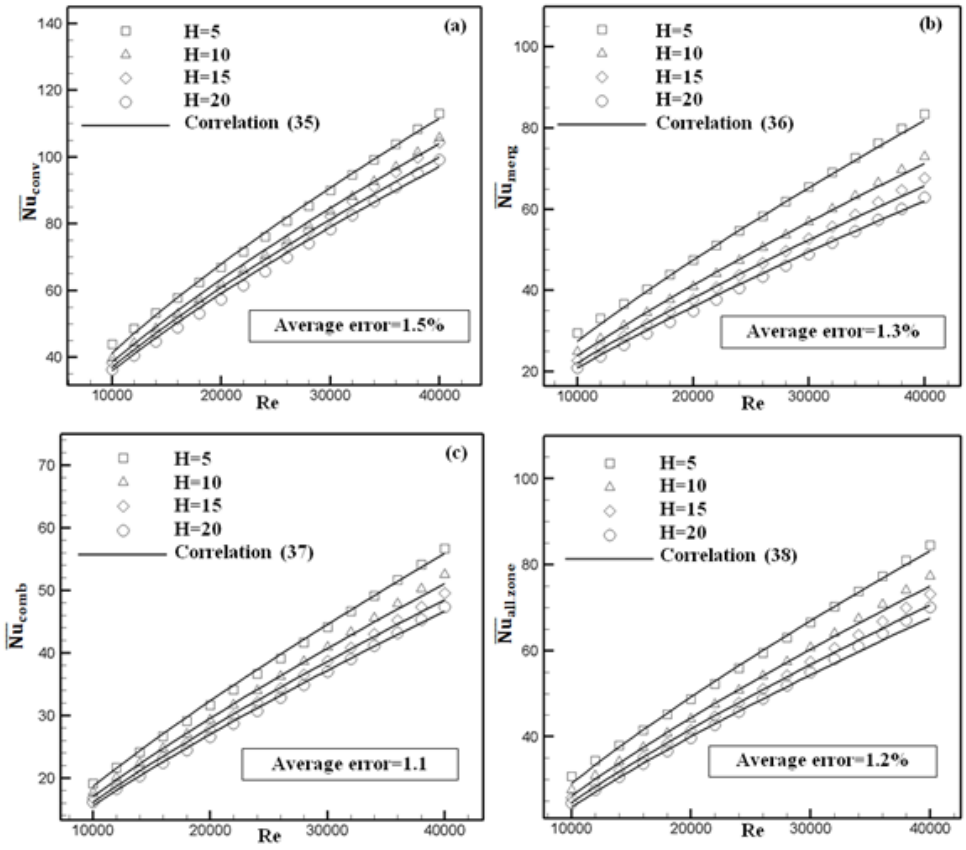

Fig. 11: Validation of correlations (Eqs. (29-32)) predicting the average Nusselt number with the present numerical results (a) converging zone (b) merging Zone (c) combined zone (d) whole flow zone.

4. Conclusions

As part of the present numerical investigation, we have performed a CFD simulation of a turbulent two-dimensional WOJ flow combining a wall jet (LWJ) and an offset jet (UOJ). The main objective of this numerical study is to investigate the offset ratio H and the Reynolds number Re effect on the heat transfer phenomenon over this type of flow. The discussion focuses mainly on the validity of the standard k-ω turbulence model to predict the different dynamics and thermal characteristics of the WOJ flow. Our numerical investigation can be used for rapid estimation of these different characteristics that are so important to a better understanding of the heat transfer mechanism in the WOJ flow that is frequently encountered in various industrial and engineering applications. Some important results had been obtained through the present paper.

(1) For all considered offset ratios H, the local Nusselt number Nu increases when increasing the Reynolds number in the different WOJ flow zones (converging zone, merging zone and combined zone). In the convergence zone, and for all Re between 10000 and 40000 and H between 5 and 20 , the local Nusselt number Nu along the wall for single wall jet (SWJ) flow is greater than that for WOJ flow. For fixed Reynolds number, more the offset ratio H increases, more the Nu longitudinal distribution in the WOJ flow case approaches that of a SWJ. Increasing the offset ratio H then results in local heat transfer intensification along the convergence zone.

(2) Along the merging zone, for fixed Reynolds number and for all $5 \leq H \leq 20$, the local Nusselt number firstly longitudinally decreases then constant values of Nu appear indicating heat transfer stabilization for some longitudinal positions. For fixed Reynolds number, elevating the offset ratio H results in a local Nusselt number decrease along the merging zone.

(3) In the combined zone and for $X \leq 40$, Nu curves are almost the same for all considered offset ratios H, whereas beyond X=40, increasing the offset ratio H results in a local Nusselt number decay. This decrease in Nu for higher H values is little observed for Re=10000, while becomes accentuated when the Reynolds number increases.

(4) The average Nusselt number $\overline{Nu}$ along each flow zone (convergence zone, merging zone and combined zone) as well as along the whole WOJ flow zone increases linearly according to the Reynolds number for all

considered offset ratios H whereas for a fixed Reynolds number, $\overline{Nu}$ decreases when H. The average Nusselt number evolution along the wall, under constant heat flux, according to the offset ratio H and the Reynolds number Re is predicted by Eqs. (29-32) respectively along the converging, merging, combined zones and along the whole WOJ flow zone.

References

1. X .Wang, S. Tan, Experimental Investigation of the Interaction Between a Plane Wall Jet and a Parallel Offset Jet, Exp. Fluids, Volume, Page 551–562, 2007.
2. E. Vishnuvardhanarao, M. K. Das, Study of the heat transfer characteristics in turbulent combined wall and offset jet flows, International Journal of Thermal Sciences, Volume 48, Page 1949–1959, 2009.
3. J.R.R. Pelfrey, J.A. Liburdy, Effect of curvature on the turbulence of a two-dimensional jet, Journal of Fluid engineering. Volume 3, Page 143–9, 1986.
4. A. Kumar, Mean flow characteristics of a turbulent dual jet consisting of a plane wall jet and a parallel offset jet, Computers and Fluids, Volume 114Page 48–65, 2015.
5. T. Modal, A. Guha, M.K. Das, Effect of bottom wall proximity ion the unsteady flow structure of a combined turbulent wall jet and offset jet flow, European Journal of Mechanics B/Fluids, Volume 57, Page 101-114, 2016.
6. L. Zhiwei, H. Wenxin, H. Jie, Large eddy simulation of the interaction between wall jet and offset jet, Journal of Hydrodynamics, Volume 23, Page 544-553, 2011.
7. S. Patankar, Numerical Heat Transfer and Fluid Flow, Hemisphere, New York.
8. N. Hnaien, S. Marzouk, H. Ben Aissia, Numerical investigation of velocity ratio effect in combined wall and offset jet flows, Journal of Hydrodynamics, Accepted In Press, 2016.
9. A. Kumar, M.K. Das, Study of a turbulent dual jet consisting of a wall jet and an offset jet, J Fluids Eng, Volume 133, Page 1201-1211, 2011.
10. A. Kumar, Mean flow and thermal characteristics of a turbulent dual jet consisting of a turbulent wall jet and a parallel offset jet, Numerical heat transfer Part A, Volume 64, Page 1075-1096, 2015.
11. D.S. Kim and S.H. Yoon, Flow and heat transfer measurements of a wall attaching offset jet, Int. J. Heat Mass Transfer, Volume 39, Page 2907-2913, 1996.
12. H.B. Song, SH. Yoon, D.H. Lee, Flow and heat transfer characteristics of a two-dimensional oblique wall attaching offset jet, Int J Heat Mass Transfer, Volume 43, Page 2395–404, 2000.
13. N. Gao, D. Ewing, C.Y. Ching, Heat transfer in turbulent planar offset attaching jet with small initial offset distances, International Journal of Heat and Mass Transfer, Volume 83, Page 21-26, 2015.

Nomenclature

d	Nozzle width (m)
e	Grid expansion ratio
h	Offset ratio (m)
H	Dimensionless offset ratio H=h/d
I	Turbulence intensity (%)
k	Turbulent kinetic energy (m^2/s^2)
K	Dimensionless turbulent kinetic energy $K=k/u_0^2$
l	Nozzle length (m)
L	Horizontal wall length (m)
Nu	Local Nusselt number $Nu = \frac{\tilde{h} \times d}{\lambda}$
$\overline{Nu}$	Average Nusselt number
p	Static pressure (Pa)
P	Dimensionless static pressure $P = \frac{p - p_a}{\rho u_0^{\ 2}}$
Re	Reynolds number $Re = \frac{u_0 \times d}{\upsilon}$
s	Grid spacing
u	Longitudinal velocity (m/s)
U	Dimensionless longitudinal velocity $U=u/u_0$
x	Longitudinal coordinates (along x axis) (m)
X	Dimensionless longitudinal coordinates X=x/d
y	Transverse coordinates (along y axis) (m)
Y	Dimensionless transverse coordinates Y=y/d
$\tilde{h}$	Heat transfer coefficient ($w/m^2.k$) $h = \frac{q_w}{T_w - T_a}$
v	Transverse velocity (m/s)
V	Dimensionless transverse velocity $V=v/u_0$

Greek Symbols

μ	Dynamic viscosity (kg/m.s)
υ	Kinematic viscosity (m^2/s)
ρ	Fluid density (kg/m^3)
λ	Thermal conductivity (w/m.k)
ω	Specific dissipation rate of k (1/s)

Subscripts

0	Initial value (at the nozzle exit)
a	Ambient value
max	Maximum value
t	Turbulent value
w	Wall value

Abbreviation

WOJ	Combined wall and offset jet flow
FPJ	Free parallel jets.
LWJ	Lower wall jet
UOJ	Upper offset jet
SOJ	Single offset jet flow
UVC	Upper vortex center
LVC	Lower vortex center
MP	Merge point
CP	Combined point
conv	Converging zone
merg	Merging zone
comb	Combined zone
all.zone	Along the whole WOJ zone